Journal of Materials Chemistry A

Accepted Manuscript

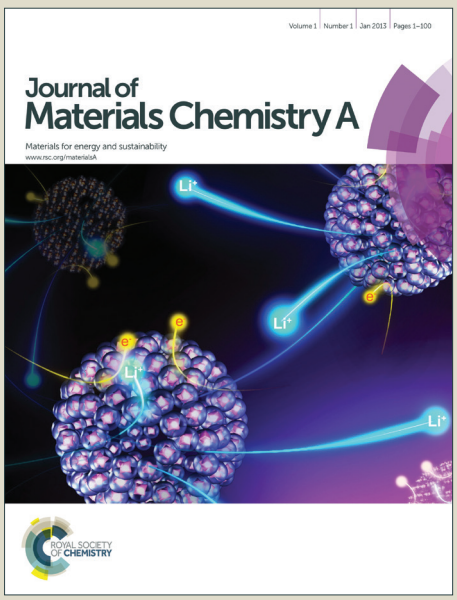

ROYAL SOCIETY OF CHEMISTRY

www.rsc.org/materialsA

Panchromatic Ru(II) Sensitizers Bearing Single Thiocyanate for High Efficiency Dye Sensitized Solar cells

Sheng-Wei Wang,[a] Chun-Cheng Chou,[a] Fa-Chun Hu,[a] Kuan-Lin Wu,[a] Yun Chi,[a,*] John N. Clifford,[b] Emilio Palomares,[b,c] Shih-Hung Liu,[d] Pi-Tai Chou,[d,*] Tzu-Chien Wei[e,*] and Ting-Yun Hsiao[f]

[a] Department of Chemistry and Low Carbon Energy Research Center, National Tsing Hua University, Hsinchu 30013, Taiwan; E-mail: ychi@mx.nthu.edu.tw

[b] Institute of Chemical Research of Catalonia, Avda. Països Catalans 16, Tarragona E-43007, Spain

[c] ICREA, Passeig Lluís Companys 28, Barcelona E-08030, Spain

[d] Department of Chemistry and Center for Emerging Material and Advanced Devices, National Taiwan University, Taipei 10617, Taiwan; E-mail: chop@ntu.edu.tw

[e] Department of Chemical Engineering, National Tsing Hua University, Hsinchu 30013, Taiwan; E-mail: tcwei@mx.nthu.edu.tw

[f] Department of Engineering and System Science, National Tsing Hua University, Hsinchu 30013, Taiwan

---

Abstract

We report on a new series of Ru(II) sensitizers PRT-21 ~ PRT-24 suitable for high performance dye sensitized solar cells (DSCs). Their molecular design consists of a tridentate anchor, a bidentate pyrazolate ancillary and a single thiocyanate. On this architecture, we examined two types of anchor incorporating the traditional 4,4'4"-tricarboxy-2,2':6',2"-terpyridine (i.e. tctpy) and newly evaluated 4,4'-dicarboxy-6-quinolin-8-yl-2,2'-bipyridine (i.e. Qbpy). This modification, together with the synergistic incorporation of either 5-hexylthien-2-yl or

5-(hexylthio)thien-2-yl substituent at the 4-position of the pyridyl pyrazolate chelate for enhancing the optical response, leads to the achievement of DSC with a prominent J_{SC} of 20.4 mA·cm^{-2} and V_{OC} = 740 mV, and hence a high photon conversion efficiency of 11.16% using PRT-22. Comprehensive charge extraction, transient photovoltage and transient absorption measurements have been carried out to gain insight into the fundamental of these new dyes and the associated device properties. These panchromatic Ru(II) sensitizers offer better product yields, higher stability and lower synthetic costs versus that of black dye (N749), adding another dimension for better sensitizers en route to high performance DSCs.

TOC illustration:

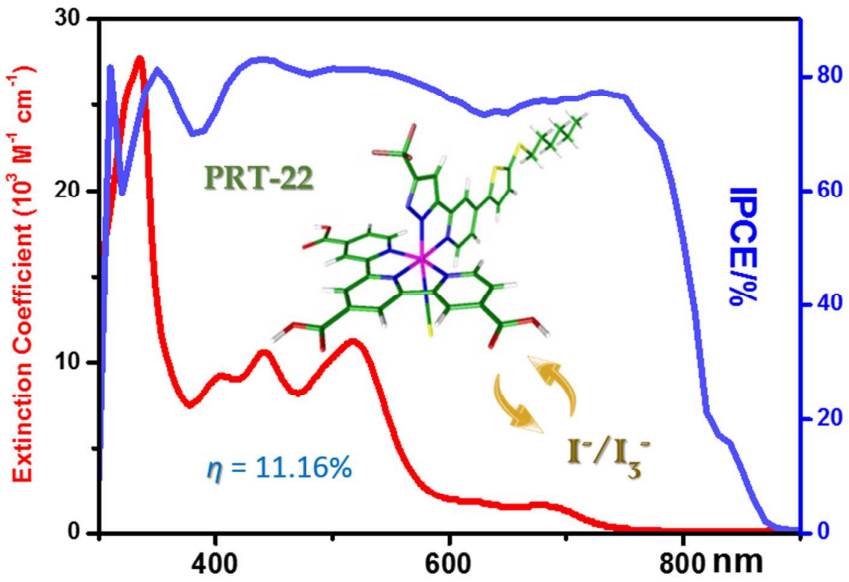

1. Introduction

Dye-sensitized solar cells (DSCs) are alternative photovoltaic devices due to the lower material costs and attractive unique features such as viable modification of color and transparency.[1, 2] In recent days, the overall performances of DSCs have

been extensively improved by fine-tuning both the morphology and hierarchical architecture of TiO_2 nanoparticles and the associated photoanodes.[3, 4] Furthermore, a decent photo-sensitizer can effectively improve the light harvesting and electron injection efficiencies and, hence, is pivotal to the success of this technology. The commonly employed sensitizers include organic dyes,[5-9] zinc prophyrin[10-12] and Ru(II) based organometallic sensitizers.[13-15] Grätzel, Nazeeruddin and coworkers had reported the seminal work on the Ru(II) sensitizer $[Bu_4N]_3[Ru(Htctpy)(NCS)_3]$, also known as N749 or black dye (Chart 1).[16]

Meanwhile, the rapid progression of another class of dye sensitized solar cells, namely: pervoskite cells should be noticed,[17, 18] for which a certified efficiency of 16.2% was recently achieved.[19] Nevertheless, the health hazard of lead pervoskite remains a critical issue that may undermine its future employment. This dilemma encourages scientists to continuously stay on the track of traditional DSCs. In this regard, Ru(II) based DSCs are fabricated using the environmental benign materials, and have achieved a record high conversion efficiency of up to 12.0% with the employment of N749 and organic co-sensitizers; the latter is essential for offsetting the strong competitive absorption of I^-/I_3^- couple of electrolyte.[20] Parallel to these studies, many efforts have also been made focusing on the optimization of molecular design of N749. Accordingly, Han,[21] Chi,[22] and Kimura and coworkers[23] independently reported the modification of 4,4'4"-tricarboxy-2,2':6',2"-terpyridine (i.e. tctpy) anchor by the removal of one carboxy group from the terminal pyridine and incorporation of a moderately electron-donating 4-methylstyryl or functionalized 2-hexylthienyl appendage, giving complexes such as HIS-2 and PRT-12 shown in Chart 1. Notably, DSC cells fabricated with these sensitizers exhibited outstanding photovoltaic performance with the highest efficiency of ~11.1%.[21]

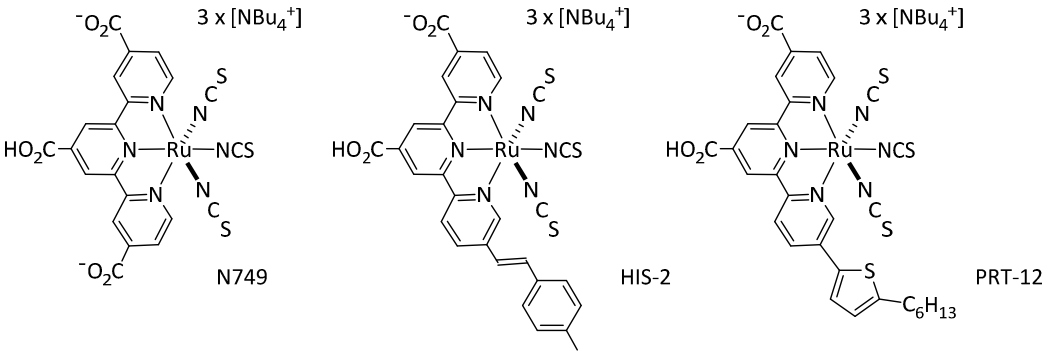

Chart 1. Structural drawings for N749, HIS-2 and PRT-12.

Alternatively, it has been suggested that Ru(II) sensitizers with all chelating (or multi-dentate) ligands can attain better sensitizer stability and longer device lifespan in comparison to those possessing more than one thiocyanate (or isothiocyanate).[24, 25] This has initiated studies on the new Ru(II) sensitizers bearing the abovementioned tridentate anchor plus a second tridentate ancillary, which has the capability in fine-tuning both the electrochemical potentials and photophysical properties for achieving better coverage of solar spectrum and hence the light harvesting efficiency.[26] Representative designs of such heteroleptic bis-tridentate sensitizers, i.e. TF-3,[27] RuNCN[28] and TF-32,[29] are depicted in Chart 2, among which the best reported efficiency is ~10.7% for TF-3 (R = 5-hexyl-(EDOT)).

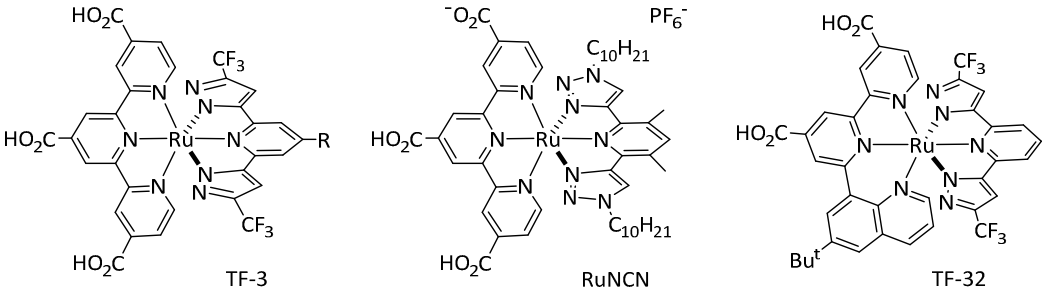

Chart 2. Structural drawings for TF-3, RuNCN and TF-32.

Despite of the conceptual triumph in this class of "thiocyanate-free" Ru(II) sensitizers, there are documents to confirm that the sulfur atom of coordinated

thiocyanate ligand is able to make intimate contact with iodide based redox couple in electrolytes, such that the regeneration of oxidized sensitizers can be rapidly achieved.[30-34] This belief initiated the evaluation of Ru(II) sensitizers bearing a single thiocyanate ligand, such that a compromise between rapid sensitizer regeneration and better stability for the sensitizers devoid of thiocyanate could be realized.[35-38] Accordingly, progresses in optimization of sensitizers were made through controlling the electrochemical potentials, increasing the optical cross section and expanding light absorption capability.[39-41] In this approach, representative sensitizers PRT-4[42] and FT89[43] are depicted in Chart 3, and the highest efficiency for the fabricated solar cells climbs to approx. 10.7%.[43]

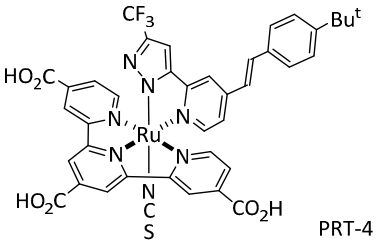

PRT-4

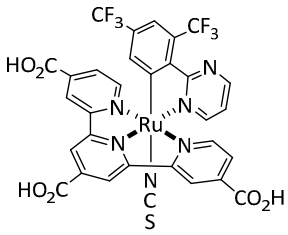

FT89

Chart 3. Structural drawings for PRT-4 and FT89.

In an aim to achieve even higher efficiency, we report here the strategic design and syntheses of a new series of panchromatic Ru(II) terpyridine sensitizers PRT-21 ~ PRT-24 (Chart 4), which possess two distinctive thienyl functionalized pyridine pyrazolate (pypz) chelates, together with either tridentate tctpy or Qbpy anchor.[29] By using bidentate pypz in substitution for two thiocyanates, these new sensitizers (with either tctpy or Qbpy anchor) exhibit significantly higher molar extinction coefficients at 400 – 550 nm versus their reference complexes, i.e. N749, PRT-4 and FT89. This enhancement in optical response, together with the extension of the absorption onset toward > 800 nm, leads to better light-harvesting capability across visible and near infrared (NIR) region, giving superior performance for the as-fabricated DSC cells.

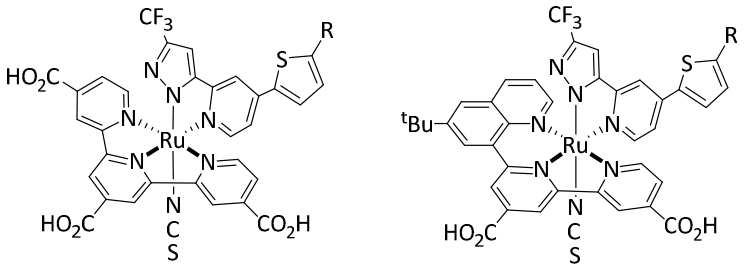

PRT-21, R = C_6H_{13}
PRT-22, R = SC_6H_{13}

PRT-23, R = C_6H_{13}
PRT-24, R = SC_6H_{13}

Chart 4. Structural drawings for PRT-21 – 24.

2. Experimental section

General Procedures. All reactions were performed under nitrogen. The required azolate ancillaries were synthesized according to the literature methods.[44] All reactions were monitored by TLC with pre-coated silica gel plates (Merck, 0.20 mm with UV254 indicator). Column chromatography was carried out using silica gel obtained from Merck (230 - 400 mesh). Mass spectra were obtained on a JEOL SX-102A instrument. ^1H and ^{19}F NMR spectra were recorded on a Bruker-400 or INOVA-500 instrument. Elemental analysis was carried out with a Heraeus CHN-O Rapid Elementary Analyzer. Photophysical data were obtained using an Edinburgh Fluorescence spectrometer FLS928P.

Synthesis of PRT-22. A mixture of (tectpy)$RuCl_3$ (100 mg, 0.14 mmol), 4-(5-(hexylthio)thien-2-yl)-2-(3-(trifluoromethyl)-1H-pyrazol-5-yl)pyridine (62 mg, 0.15 mmol), and KOAc (30 mg, 0.3 mmol) in 30 mL of toluene was heated to reflux for 6 h. After evaporating the solvent, the residue was purified by silica gel column chromatography (CH_2Cl_2/ethyl acetate = 10:1). After then, this solid material was mixed with KSCN (111 mg, 1.1 mmol) in 30 mL of DMF and the solution was heated to reflux for 2 h. The solvent was removed and the residue was purified by silica gel column chromatography (CH_2Cl_2/ethyl acetate = 10:1), The obtained solid was then dissolved in a mixture of acetone (30 mL) and 2 M NaOH solution (2 mL) and stirred at room temperature overnight. Finally, the solution was concentrated, and the solid

dissolved in 10 mL of H_2O and titrated with 2 N HCl to pH 3 to afford a black precipitate. It was then washed with H_2O, acetone and diethylether in sequence, yielding PRT-22 (54 mg). The synthetic procedures for other Ru(II) sensitizers, i.e. PRT-21, PRT-23 and PRT-24, and the corresponding spectral and analytical data are depicted in the supporting information.

Spectral data of PRT-22: MS (FAB, ^{102}Ru): m/z 935 $(M+1)^+$. ^{1}H NMR (400 MHz, d_6-DMSO, 298 K): δ 9.25 (s, 2H), 9.23 (s, 1H), 9.11 (s, 2H), 8.46 (s, 1H), 8.06 ~ 8.03 (m, 4H), 7.83 (dd, J_{HH} = 7.4, 1.6 Hz, 2H), 7.37 (d, J_{HH} = 3.8 Hz, 1H), 7.24 (s, 1H), 3.01(t, J_{HH} = 7.2 Hz, 2H), 1.68 ~ 1.61 (m, 2H), 1.43 ~ 1.26 (m, 6H), 0.87 (t, J_{HH} = 6.8 Hz, 3H). Anal. Calcd for $C_{38}H_{30}F_3N_7O_6RuS_3 \cdot H_2O$: C, 47.89; N, 10.29; H, 3.38. Found: C, 47.84; N, 10.16; H, 3.71.

TD-DFT Calculation. All calculations were performed by Gaussian 09 program. Their ground state structures were first optimized with density functional theory (DFT) at B3LYP/LANL2DZ (Ru) and 6-31G* (H, C, N, O, F) level. The optimized structures were then used to calculate 60 lowest singlet energy optical excitations using the time-dependent density functional theory (TD-DFT) method. Also calculated were their lowest ground triplet state energies. To mimic the solution phase a polarizable continuum model (PCM) in Gaussian 09 was applied using dimethylformamide (DMF) as the solvent.

Device fabrication. The pre-cleaned FTO glasses (4 mm thickness, Nippon Sheet Glass Co., Japan) were immersed into a 40 mM aqueous $TiCl_4$ solution at 70 °C for 30 min and washed with water and ethanol. It was then deposited with a 15 μm of TiO_2 electrode, followed by a 7 μm scattering layer containing 400 nm TiO_2 particles (PST-400, JGC Catalysts and Chemicals, Japan). The TiO_2 electrodes were heated in air at 325 °C for 30 min, followed by heating at 375 °C for 5 min, 450 °C for 15 min, and 500 °C for 30 min. The TiO_2 electrodes were treated with a 40 mM aqueous solution of $TiCl_4$ for 30 min at 70 °C followed by heating again at 500 °C for 30 min. After then, these TiO_2 films were dipped in 0.1 M HCl solutions in ethanol for 2h followed by

washing with water and ethanol and dried under a N_2 flow,[45] before treatment with a dye solution for 18h at 25 °C, which were prepared using absolute ethanol and *t*-butanol (v/v, 1:1).

Dye solution contains 0.3 mM of each sensitiser, together with 0.6 mM of tetra-butylammonium deoxycholate [TBA][DOC] and 1 mM deoxycholic acid (DCA) as co-adsorbate. The counter electrodes were coated with a thin layer of the PVP capped platinum nanoclusters (PVP-Pt) via a so-called "two-step dip coating" process on FTO glass (7Ω/TEC7, 2.2 mm thick, Pilkington), followed by a post heating at 325 °C for 10 min.[46] The electrodes were assembled by inserting a hot-melt Surlyn film (Meltonix 1170-25, 25 μm, Solaronix), and heated at 130 °C. The electrolyte composed of 0.6 M 1,2-dimethyl-3-propylimidazolium iodide (DMPII), 0.1 M lithium iodide, 0.05 M iodine, 0.1 M guanidinium thiocyanate (GuNCS), and 0.5M *t*-butylpyridine (tBP) in acetonitrile. It was then injected into the cell through a pre-drilled hole at the counter electrode.

3. Results and Discussion

Synthesis and structural characterization. The syntheses of the Ru(II) sensitizers PRT-21 – PRT-24 are given in the experimental section and Electronic Supporting Information (ESI). Two functionalized pyridyl azolate ancillaries, each with different appendage attached at the 4-position of pyridyl group, i.e. R = 5-hexylthien-2-yl and 5-(hexylthio)thien-2-yl, were selected for probing their influence on the UV-Vis spectra, and photovoltaic properties. The corresponding ester derivatives were prepared by reacting $RuCl_3 \cdot 3H_2O$ with 4,4'4"-triethoxycarbonyl-2,2':6',2"-terpyridine (tectpy)[16] or with diethyl 6-(6-(t-butyl)quinolin-8-yl)-[2,2'-bipyridine]-4,4'-dicarboxylate (Et-Qbpy),[29] followed by treatment with the respective 2-pyridyl azoles. The crude ethoxycarbonyl substituted Ru(II) intermediates were isolated by silica gel column chromatography, treated with KSCN and a second run of chromatographic purification. Finally, the ethoxycarbonyl groups were hydrolyzed in the mixture of

acetone and 2M NaOH solution at room temperature. The resulting Ru(II) sensitizers PRT-21 ~ PRT-24 were precipitated by adjusting to pH = 3, followed by rinsing with water, acetone and diethylether in sequence, and extensive drying under vacuum.

Photophysical behaviors. The absorption spectra of PRT-21 – PRT-24 were recorded in DMF at a concentration of 1 x 10^{-5} M, which are depicted in Figure 1, while their numeric and electrochemical data are summarized in Table 1. These PRT sensitizers all display a broad, multiple absorption band extended to ~800 nm. Upon anchored to the TiO_2 surface, all four spectra showed increase in absorption strength, especially at the red edge. This is attributed to the increase of dye concentration and caused the relatively absorptivity on TiO_2 being greater than the spectral profile recorded in solution. Notably, for PRT-23 and PRT-24 with Qbpy anchoring group, their absorptivity in the range of ~430 – 600 nm is in general more intense than that of the PRT-21 and PRT-22 with the tctpy anchor. This general trend is attributable to a result of larger π-conjugation for quinoline (in the Qbpy anchor) versus pyridine (in the tctpy anchor) and hence a better absorptivity as a result of higher density of states and hence the greater transition moment in this region (vide infra). Despite of the more intense absorptivity in general, however, the spectral onset of PRT-23 and PRT-24 seems to be higher in energy, i.e., shorter in wavelength, than that of PRT-21 and PRT-22 (Figure 1). This puzzle may be rationalized by the difference in number of carboxylic anchoring groups among these dyes.[47] The carboxylic substituent acts as an electron withdrawing substituent, which lowers the LUMO energy level of all pyridyl moieties in tctpy chelate of PRT-21 and PRT-22, consequently decreasing the energetics of the lowest lying electronic transition. In comparison, the quinolinyl substituent in PRT-23 and PRT-24 was intentionally designed to have one less carboxylic anchoring group, so that it acts as better antenna to harvest light in the visible region.[29] In other words, the quinoline moiety in PRT-23 and PRT-24 may not participate in LUMO in their lower lying transition.

The above viewpoints are supportive by the corresponding TD-DFT calculation, in which the lowest lying singlet excited state (S_1) of PRT-21, 22, 23, and 24 are calculated to be at 738, 738.2, 701.8, and 703 nm, respectively (see Table S1 – S4, ESI). Additionally, the energetics of lowest triplet state (T_1) are calculated to be 812.8 nm (PRT-21), 813.1 nm (PRT-22), 784.8 nm (PRT-23) and 785.4 nm (PRT-24). Therefore, the lowest lying electronic transition for PRT-21 and PRT-22 is lower than that of PRT-23 and PRT-24 in both singlet and triplet manifolds. Note that the calculated $S_0 \rightarrow T_1$ transition (oscillator strength) is null in the current calculation, that is, a strictly forbidden singlet-triplet conversion under zeroth-order approximation.[48] In reality, however, the $S_0 \rightarrow T_1$ transition of the titled Ru(II) complexes is partially allowed due to the spin-orbit coupling and small S_1-T_1 energy gap, giving the non-negligible transition moment based upon the first-order perturbation theory.[49] The combination of $S_0 \rightarrow S_1$ and $S_0 \rightarrow T_1$ transition rationalizes the experimentally observed spectral onset toward ~800 nm for the titled compounds. Careful frontier orbital analyses (see Table S1 – S4 and Figures S1 – S4 in ESI) indicate that both S_1 and T_1 can be described by mainly HOMO $\rightarrow$ LUMO transition incorporating the metal-to-ligand charge transfer (MLCT) and ligand-to-ligand charge transfer (LLCT) originating from the pyrazolate ancillary to the anchor. In consistence with the experimental viewpoint, the quinoline moiety in PRT-23 and PRT-24 does not contribute to the lowest lying transition but rather involves in the higher lying electronic transition in the region of 450 – 650 nm described below.

As for the higher lying electronic states, we then compare the experimental spectra and the calculated vertical oscillator strengths for all titled complexes, which are gathered in Figure 2 (for PRT-22 and PRT-24) and Figure S5 (for PRT-21 and PRT-23). As for PRT-21 and PRT-22, their spectral maxima in the region of 450 – 650 nm are located at ~520 nm and the corresponding calculated peaks are at 531 and 531.1 nm ($S_0 \rightarrow S_4$), respectively, which are mainly ascribed to MLCT from the Ru

metal to tctpy moiety (see Figure S5a and Figure 2a) and partly LLCT from pyrazolate and thiocyanate to tctpy. For PRT-23 and PRT-24, their experimental peaks wavelength in the range of 450 – 650 nm are located at ~537 nm and the corresponding calculated peaks are at 521.9 and 522.3 nm ($S_0 \rightarrow S_4$), respectively, which can be well described by a combination of MLCT (Ru $\rightarrow$ Qbpy) and LLCT (pyrazolate and thiocyanate $\rightarrow$ Qbpy) (see Figure S5b and Figure 2b). The involvement of quinoline moiety rationalizes the higher absorptivity for PRT-23 and PRT-24 (cf. PRT-21 and PRT-22) in the spectral region of 450 – 650 nm. The spectra in the region of 400 – 450 nm are mainly ascribed to both the MLCT and ILCT transitions involving the ancillary ligand, i.e. the 5-hexylthien-2-yl (for PRT-21 and PRT-23) or 5-(hexylthio)thien-2-yl (for PRT-22 and PRT-24) substituted pyridyl pyrazolate (see Figure 2). The distributions of the calculated oscillator strengths of each titled complex in comparison to the corresponding experimental absorption spectra are qualitatively in the same trend, although not in exact match with each other. We believe that this is due to the computational errors under B3LYP/6-31G*/LANL2DZ functional/basis set in general. Lastly, it is noted that the thiocyanate shows substantial contribution in HOMO among all titled complexes. Thus, upon excitation, the dye regeneration can take place here by accepting electron from iodide in electrolyte.[50] Therefore, thiocyanate should facilitate the regeneration of the oxidized sensitizer, hence improving the DSC performance. Alternatively, the presence of a single thiocyanate also limited the number of sulfur atom (versus two thiocyanates in N719 and C106) that can interact with iodine (or triiodide) in the same electrolyte,[51-53] resulting in a slower charge recombination and, hence, higher device efficiency.

In sharp contrast, the absorption spectra of tctpy sensitizers PRT-21 and PRT-22 on a 6 μm TiO_2 thin film are notably more intense than that of Qbpy sensitizers PRT-23 and PRT-24 at the shorter wavelength region. This reverse in absorptivity also occurs at the longer wavelength region of 630 – 800 nm. Such a remarkable result is

attributed to the larger dye loading for the tctpy analogues PRT-21 and PRT-22 (see Table 2). Besides, upon substitution of 5-hexylthien-2-yl with 5-(hexylthio)thien-2-yl appendage, the respective PRT-22 and PRT-24, irrespective to the anchoring group, displayed notable red-shifting and more intense LLCT and MLCT absorptions, for which similar effect has been observed for the pairs of Ru(II) sensitizers C106 and C101[54] and TFRS-62 and TFRS-63.[55]

Electrochemical properties. Cyclic voltammetry was measured for calculating the ground and excited-state oxidation potentials ($E^{0\prime}$ and $E^{0\prime}$*) of these PRT sensitizers. As shown in Table 1, the ground-state oxidation potentials of PRT-21 to PRT-24 appeared in the range 0.85 –0.97 V (vs. NHE), which are more positive than that the I^-/I_3^- redox couple (ca. 0.4 V vs. NHE), confirming the existence of sufficient driving force for dye regeneration.[56-58] Moreover, the excited-state oxidation potentials were next estimated from the difference of $E^{0\prime}$ and the optical bandgap (i.e. from intersection of the lowest energy UV/Vis absorption and PL emission peaks), are also more negative than the conduction band edge (CB) of the TiO_2 electrode (ca. −0.5 V vs. NHE), confirming the existence of good driving force for effective electron injection.

Device performance characteristics. The IPCEs of as-fabricated cells are shown in Figure 3a, for which the action spectra can be classified into two groups based on their carboxy anchor. For the tctpy sensitizers PRT-21 and 22, the onset of the IPCE action spectra started at ~860 nm and rapidly increased to 55% at 800 nm. Excellent IPCE performances of over 75% were observed starting at 730 nm, showing an even higher value upon moving to the shorter wavelength. Particularly for PRT-22, the IPCE goes up to ~80% at 730 nm, which could be attributed to the 5-(hexylthio)thien-2-yl group introduced to this sensitizer.[54]

In comparison, the onset of IPCE for the Qbpy sensitizers PRT-23 and PRT-24 is blue shifted to 820 nm, with a difference as large as 40 nm. Their IPCEs slowly raise to over 70% at 710 nm, and continuously increase to over 80% for PRT-24 and 85%

for PRT-23, both at 560 nm, for which their maxima values are notably higher than their tctpy counterparts. Furthermore, the higher IPCE profile for PRT-24 over that of PRT-23 is again attributed to the extra sulfur atom that attached at the terminal hexyl chain. The overall trends of IPCE clearly reveal that the tctpy sensitizers PRT-21 and PRT-22 exhibit better spectral response at the longer wavelength region, while their Qbpy counterparts PRT-23 and PRT-24 display superior spectral response at the shorter wavelength region of < 600 nm. The cause for such notable distinction in IPCE action spectra seems to be consistent with the UV/Vis spectral behavior discussed in the previous section.

The I-V characteristics are depicted in Figure 3b. As can be seen, tctpy sensitized solar cells gave J_{SC} = 19.0 and 20.4 mA·cm^{-2}, V_{OC} = 760 and 740 mV, and FF = 0.749 and 0.739, corresponding to an overall efficiency η = 10.81 and 11.16% for PRT-21 and PRT-22, respectively. Alternatively, the Qbpy sensitizers PRT-23 and PRT-24 revealed slightly lower current density, 18.7 and 20.2 mA·cm^{-2}, which might be due to the combination effect of higher and lower IPCE at the shorter and longer wavelength regions, respectively. Furthermore, despite of the increase in J_{SC}, there are minor reduction in the V_{OC} values for PRT-22 and PRT-24 with respect to PRT-21 and PRT-23, respectively. The corresponding V_{OC} difference was likely correlated with the formation of non-negligible sulfur-iodine (or tri-iodide) interaction between the sensitizer and electrolyte, the result of which then leads to the acceleration of electron recombination.[51, 59, 60]

As for the reference, the N749 sensitizer gave J_{SC}, V_{OC}, and fill factor (FF) of 17.7 mAcm^{-2}, 720 mV, and 0.722, corresponding to an efficiency of 9.20%, which is notably lower than that of the champion cells reported in literature.[61-63] Such a difference is apparently caused by the reduced TiO_2 thickness (15 μm) for cell fabrication, as N749 required much thicker TiO_2 layer in fabrication of optimized cells due to the reduced optical response. In sharp contrast, all our PRT sensitizers showed higher current densities (18.7 – 20.3 mAcm^{-2}) than N749 (17.7 mAcm^{-2}) with this

thinner TiO_2 layer, reflecting the advantage of added π-conjugated appendages. Integration of the IPCE spectrum with the AM1.5G solar photon flux yields a current density of 20.96 $mAcm^{-2}$ for PRT-22, which is in excellent agreement with the measured photocurrent density, extrapolated to 20.4 $mAcm^{-2}$ under the standard solar AM1.5G intensity of 100 $mWcm^{-2}$ (See Figure S6). All other IPCE action spectra also fitted very well to the respective I-V measurements.

Photophysical measurements of DSC devices. It has been reported that the photovoltage differences between these devices are due to both shifts in the CB edge of TiO_2 and differences in TiO_2 electron lifetimes, which can be gauged using charge extraction (CE) and transient photovoltage (TPV) measurements. The CE and TPV data for devices composed of these PRT sensitizers are shown in Figure 4, all with very similar distribution of electron density, together with only small differences being noted at V > 0.6 V. The electron lifetimes were next measured at identical electron densities using TPV measurement. Although the PRT-22 device has the relatively longest electron lifetime owing to the lower charge recombination, the fact that its CB is shifted further downwards as compared to the other devices explains why its V_{OC} value is comparable to that of the PRT device having shorter electron lifetime. Moreover, compared to PRT-21 and PRT-23, the V_{OC} is lower with both PRT-22 and PRT-24 due to the introduction of 5-(hexylthio)thien-2-yl substituent to the chelating pyrazolate. The difference was explained by the increased iodine or tri-iodide binding ability in view of the fact that it is the oxidized sensitizer that directly interacts with the redox mediator, leading to faster charge recombination.[51, 64] The IMPS and IMVS were also conducted and analyzed. However, the obtained electron diffusion coefficient (D) versus Jsc and electron lifetime versus voltage data are only shown in the Figure S7 of ESI as they duplicate the information produced by the CE and TPV measurements, which remained to be the major focus of the present contribution.

Transient absorption measurements, which revealed electron transfer reactions occurring at the TiO_2/dye/electrolyte interface in DSC devices, were also investigated in the presence and absence of electrolyte and the results are shown in Figure S8. All PRT-21 – PRT-24 devices display similar kinetic trace profiles and dispersive kinetics in the absence of electrolyte (black), which vary from 0.3 to 8 ms and show the bi-phasic kinetics in the presence of electrolyte (red). The fast part of these kinetics is several orders of magnitude faster than charge recombination in the absence of I^-/I_3^- redox mediator. These kinetics indicate that all PRT-21 – PRT-24 devices show regeneration kinetics closely resembling that of both N3 and N719 as measured in previous studies,[65] but the regeneration is faster than typical "thiocyanate-free" Ru(II) sensitizers that lacked the proposed sulfur-iodine contact.[66]

Electrochemical impedance spectroscopy (EIS) measurement. To clarify the governing factors on the photovoltaic performances of DSC devices, EIS were also conducted on all the PRT devices at different bias in dark. The EIS data was then analyzed using transmission line model (TLM) developed by Bisquert and co-workers.[67] The relationship between chemical capacitance (C_μ) and applied bias (V_{app}) as well as TiO_2/dye/electrolyte interfacial charge transfer resistance (R_{CT}) and applied bias are shown in Figure 5. It can be seen from Figure 5(a) that DSC composed of PRT-22 showed relatively higher C_μ, indicating the most downward shifted CB of TiO_2 among all PRT sensitizers. The lowest CB not only facilitates charge injection from PRT-22 to TiO_2 layer, but also decreases the energy gap to the redox potential of I^-/I_3^-, rendering a highest J_{SC} and slightly lower V_{OC} in PRT-22 device. From Figure 5(b), the fact of largest R_{CT} for PRT-22 device is consistent with the finding in photophysical measurements. The longest electron lifetime of PRT-22 device is speculatively related to the highest dye loading among all fabricated devices, as the densely packed sensitizer molecules on TiO_2 surface can efficiently block the electron recombination with tri-iodide.

Stability measurement. For testing long-term stability of the as-fabricated DSCs, the electrolyte need to switch to a high boiling solvent, i.e. butyronitrile (BN).[68] The performance evolution is shown in Figure 6. Over the entire 1000h testing period at 60 °C under accelerated visible-light soaking, the photovoltaic parameters J_{SC}, V_{OC}, *FF* of PRT-22 based cell varied only slightly and the final η retained 98% of its initial value. This excellent stability indicates the potential advantage of these Ru(II) sensitizers for future commercial applications.

4. Conclusion

A new series of Ru(II) sensitizers PRT-21 ~ PRT-24 suitable for high performance DSC applications have been synthesized. The strategic design of PRT-21 ~ PRT-24 lies in two folds: i.e. (i) to gain better light-harvesting efficiency upon incorporating suitable anchoring and/or π-conjugated pendant groups, and (ii) to evaluate the DSC performance among dyes with variable number of thiocyanate pendants, in which PRT-21 ~ PRT-24 represent the cases for single thiocyanate pendant. For the former, our results indicate that replacing one carboxy substituted pyridine unit in tctpy (PRT-21 and PRT-22) by *t*-butyl substituted quinoline moiety, forming PRT-23 and PRT-24, increases the light harvesting efficiency in the visible region, but suffers a tradeoff of shortening the spectral onset wavelength and a reduced dye uptake on TiO_2 photoanode. Incorporating the 5-(hexylthio)thien-2-yl substituted ancillary afforded the improved light harvesting and overall efficiency in both designs. For the second objective, the associated single thiocyanate facilitates the regeneration of the oxidized sensitizer, due to the possible contact with the iodide in electrolytes. Alternatively, it also limited the number of sulfur atom (versus two coordinated thiocyanates in N719 and C106) that can interact with iodine (or triiodide) in the electrolyte, resulting in a slower charge recombination and, hence, higher device efficiency.

Finally, DSC device with PRT-22 sensitizer, i.e. with 5-(hexylthio)thien-2-yl appendage, showed prominent J_{SC} of 20.4 mA·cm^{-2}, V_{OC} = 740 mV and η of 11.16%. This class of sensitizer also offers better yield and lower synthetic cost versus that of N749. Moreover, with retention of 98% in conversion efficiency after 1000h (60 °C) under accelerated visible-light soaking, it added another dimension for better sensitizer en route to high performance DSCs.

5. Acknowledgment.

This work was supported by the Ministry of Science and Technology (MOST), while the computation was executed using the facility at the National Center for High-Performance Computing (NCHC), Taiwan.

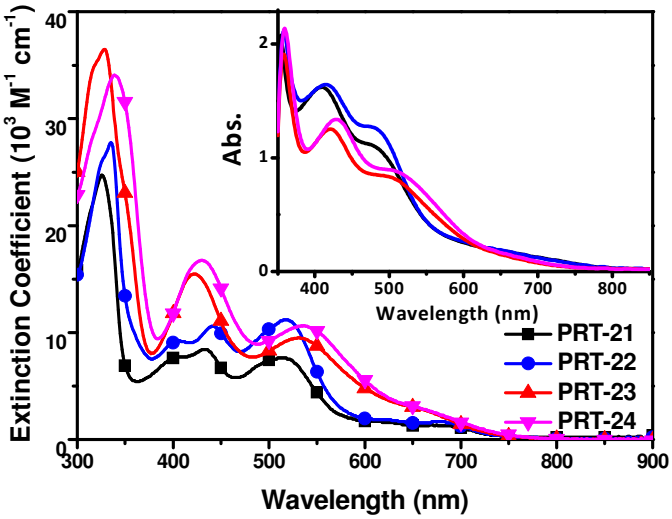

Figure 1. UV-Vis absorption spectra of PRT sensitizers in DMF. Inset: spectra of samples that adsorbed on 6 µm of transparent TiO_2 thin film.

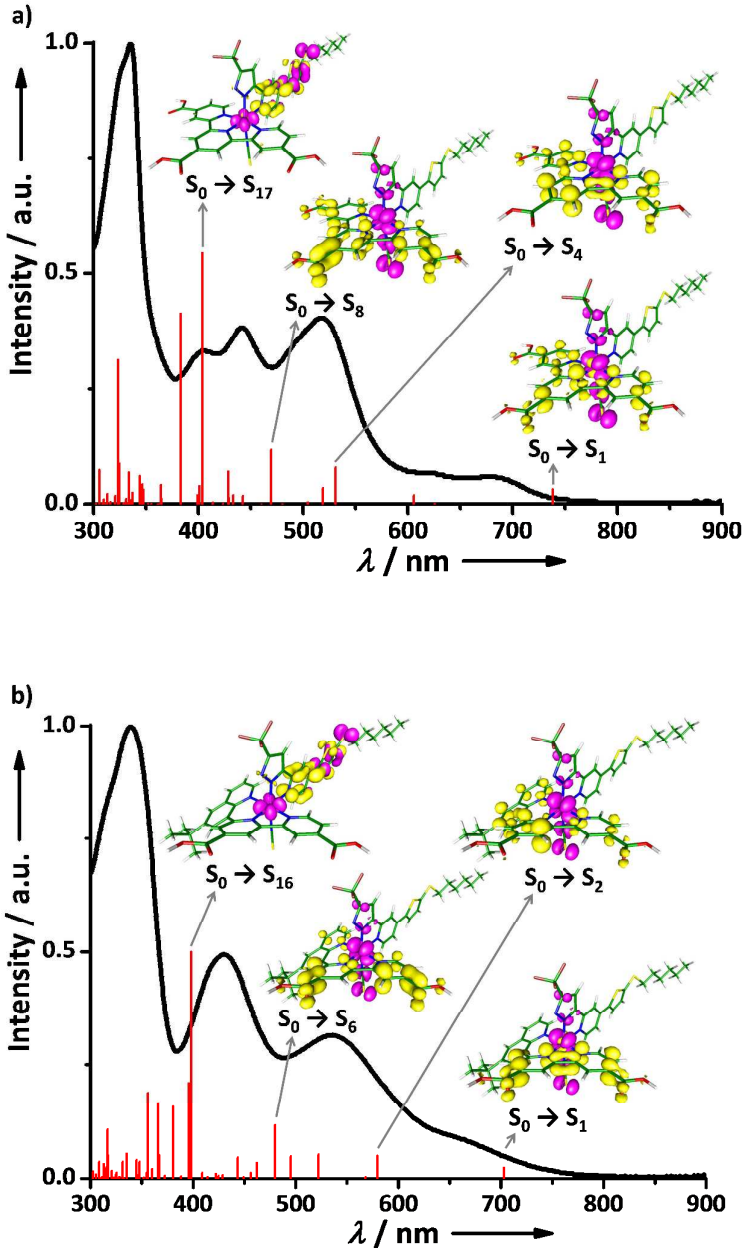

Figure 2. UV/Vis spectra and spin density plots for the specified transition of: a) **PRT-22** and b) **PRT-24**. Also depicted are the TD-DFT calculated absorption wavelengths (vertical lines) and the relative transition probability (magnitude of vertical lines). Selected frontier orbitals (pink: occupied orbital, yellow: unoccupied orbital) that contribute to the major transitions are also shown.

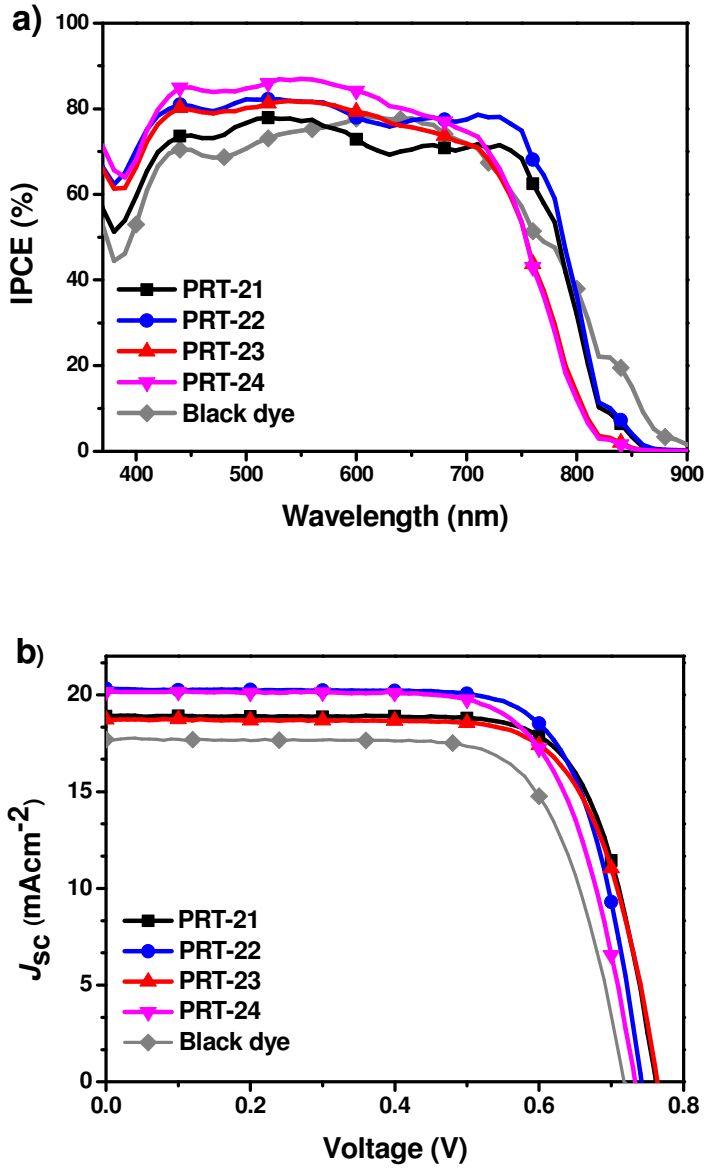

Figure 3. (a) IPCE spectra and (b) *J*-*V* characteristics measured for DSCs sensitized with various PRT sensitizers under AM1.5 solar irradiation.

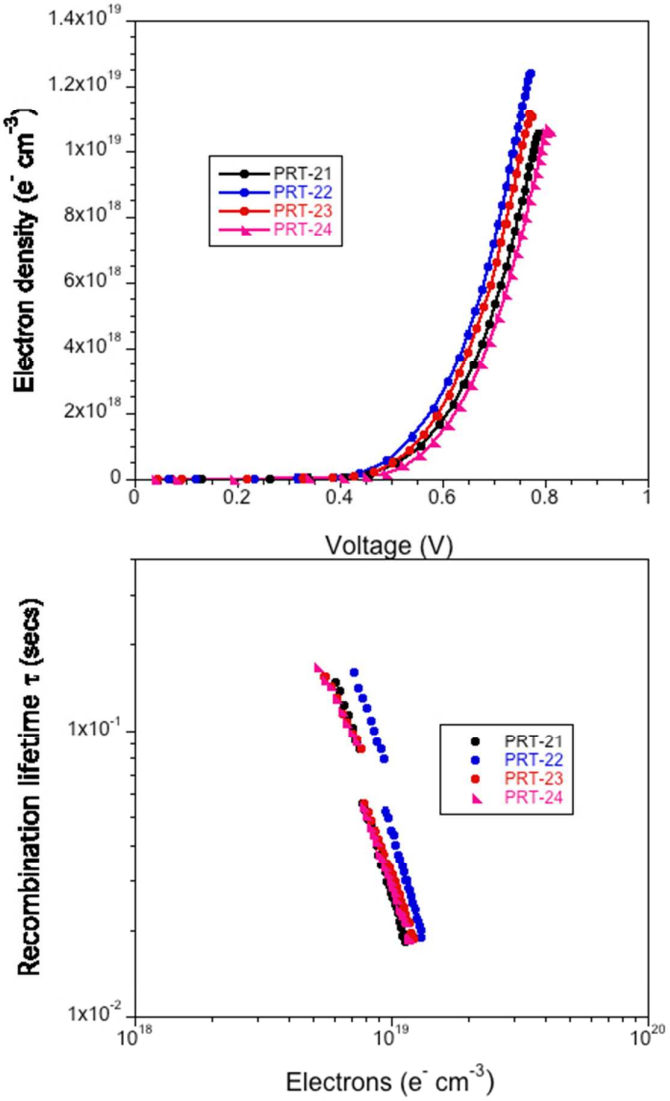

Figure 4. (a) TiO_2 electron density versus voltage deduced from charge extraction measurements and (b) electron lifetime τ versus TiO_2 electron density deduced from transient photovoltage measurements for DSC devices containing PRT sensitizers.

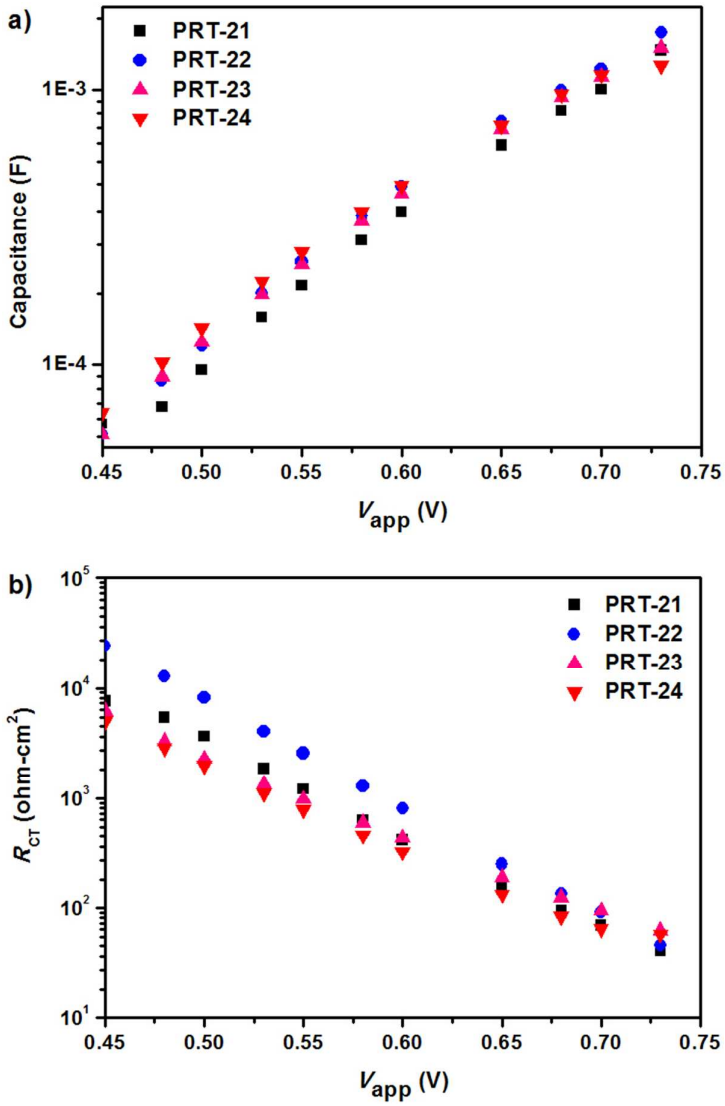

Figure 5. (a) Trend in capacitance and (b) charge transfer resistance, R_{CT}, obtained by the electrochemical impedance spectroscopy.

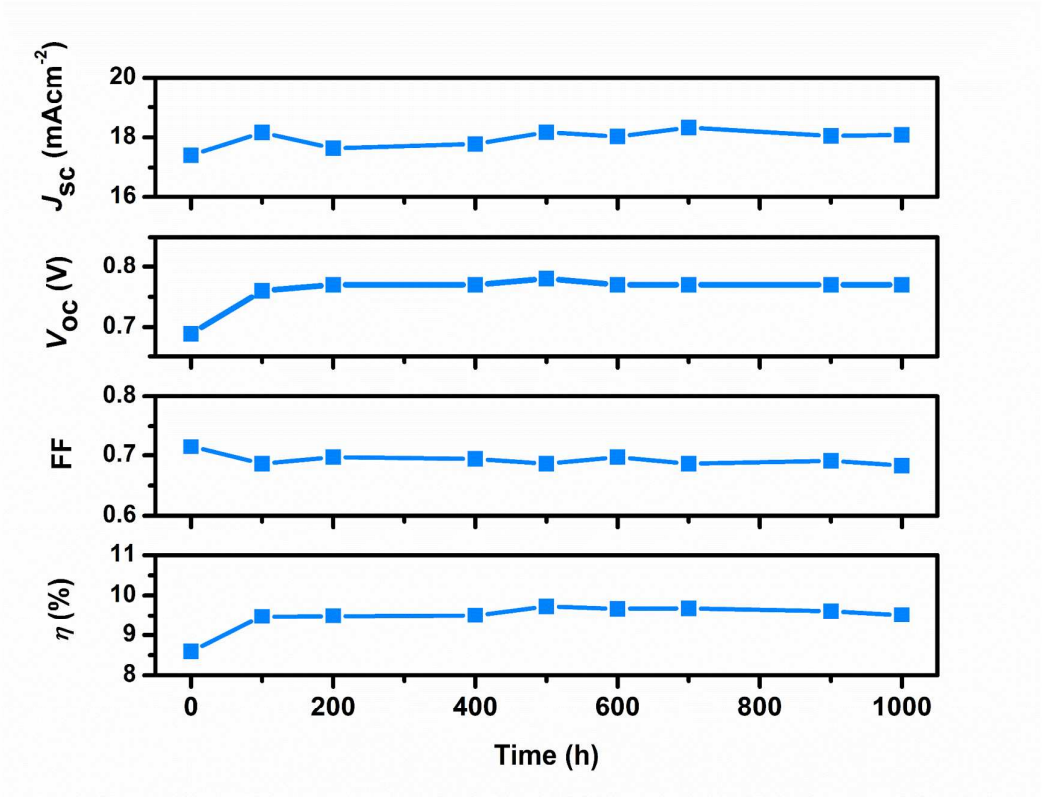

Figure 6. Evolution of solar cell parameters of PRT-22 measured under one sun light-soaking at 60 ^{o}C. Electrolyte: 0.6 M DMPII, 0.15 M I_2, 0.1 M LiI, 0.1 M GuNCS, and 0.5 M NBB (N-butyl-1*H*-benzimidazole) in butyronitrile.

Table 1. Photophysical and electrochemical data of the studied **PRT** sensitizers.[a]

sensitizer	abs. λ_{max} (nm) ($\times 10^3$ [$Lmol^{-1}cm^{-1}$])	λ_{em} (nm)	$E°'$ (V) [b]	$E_{0\text{-}0}$ (V) [c]	$E°'*$ (V) [c]
PRT-21	436 (8.4), 514 (7.6), 686 (1.3)	747	0.96	1.80	−0.85
PRT-22	442 (11), 520 (11), 684 (1.7)	757	0.97	1.81	−0.84
PRT-23	424 (15), 536 (9.5), 660 (2.8)	812	0.85	1.79	−0.94
PRT-24	431 (17), 537 (11), 660 (2.9)	805	0.86	1.80	−0.95

[a] Absorption spectra, emission peak maxima and lifetime were measured in DMF solution.

[b] Oxidation potential of dyes was measured in DMF with 0.1 M [TBA][PF_6] and with a scan rate of 50 mV s^{-1}. It was calibrated with Fc/Fc^+ as internal reference and converted to NHE by addition of 0.63 V.

[c] $E_{0\text{-}0}$ was determined from the intersection of the absorption and tangent of the emission peak in DMF. $E°'* = E°' - E_{0\text{-}0}$.

Table 2. The performances for DSCs measured under AM 1.5G one sun irradiation.[a]

Sensitizer	J_{SC} [mA·cm^{-2}]	V_{OC} [mV]	FF	η [%]	dye loading[b] [$\times 10^{-7}$ mol·cm^{-2}]
PRT-21	19.0	760	0.749	10.81	1.42
PRT-22	20.4	740	0.739	11.16	1.63
PRT-23	18.7	760	0.734	10.43	1.23
PRT-24	20.1	730	0.716	10.51	1.44
Black dye	17.7	720	0.722	9.201	–

[a] All devices were fabricated using 15 + 7 μm TiO_2 anodes and with an active area of 5 × 5 mm^2. Each data was the average of three individual cells. Device performances were measured using a black metal mask with an aperture area of 4 × 4 mm^2. [b] The loading is calculated from the MLCT band ratio for desorbed dye solution versus (0.01 mM) reference solution in mixed MeOH and water (*v/v*, 1:1) with addition of 0.1 M of [TBA]OH.

References

1. M. Grätzel, *Acc. Chem. Res.*, 2009, **42**, 1788.
2. S. Zhang, X. Yang, Y. Numata and L. Han, *Energy Environ. Sci.*, 2013, **6**, 1443.
3. J.-W. Shiu, Z.-J. Lan, C.-Y. Chan, H.-P. Wu and E. W.-G. Diau, *J. Mater. Chem. A*, 2014, **2**, 8749-8757.
4. S. S. Mali, H. Kim, C. S. Shim, P. S. Patil, J. H. Kim and C. K. Hong, *Sci. Rep.*, 2013, **3**, 3004.
5. Y. Ooyama and Y. Harima, *Eur. J. Org. Chem.*, 2009, 2903.
6. Y.-S. Yen, H.-H. Chou, Y.-C. Chen, C.-Y. Hsu and J. T. Lin, *J. Mater. Chem.*, 2012, **22**, 8734.
7. M. Zhang, Y. Wang, M. Xu, W. Ma, R. Li and P. Wang, *Energy Environ. Sci.*, 2013, **6**, 2944.
8. M. Liang and J. Chen, *Chem. Soc. Rev.*, 2013, **42**, 3453.
9. Y. Wu and W. Zhu, *Chem. Soc. Rev.*, 2013, **42**, 2039.
10. A. Yella, C.-L. Mai, S. M. Zakeeruddin, S.-N. Chang, C.-H. Hsieh, C.-Y. Yeh and M. Grätzel, *Angew. Chem. Int. Ed.*, 2014, **53**, 2973-2977.
11. C.-L. Wang, J.-Y. Hu, C.-H. Wu, H.-H. Kuo, Y.-C. Chang, Z.-J. Lan, H.-P. Wu, E. Wei-Guang Diau and C.-Y. Lin, *Energy Environ. Sci.*, 2014, **7**, 1392-1396.
12. S. Mathew, A. Yella, P. Gao, R. Humphry-Baker, F. E. CurchodBasile, N. Ashari-Astani, I. Tavernelli, U. Rothlisberger, M. K. Nazeeruddin and M. Grätzel, *Nature Chem.*, 2014, **6**, 242-247.
13. P. Xie and F. Guo, *Curr. Org. Chem.*, 2011, **15**, 3849.
14. P. G. Bomben, K. C. D. Robson, B. D. Koivisto and C. P. Berlinguette, *Coord. Chem. Rev.*, 2012, **256**, 1438.
15. J.-F. Yin, M. Velayudham, D. Bhattacharya, H.-C. Lin and K.-L. Lu, *Coord. Chem. Rev.*, 2012, **256**, 3008.
16. M. K. Nazeeruddin, P. Péchy, T. Renouard, S. M. Zakeeruddin, R. Humphry-Baker, P. Comte, P. Liska, L. Cevey, E. Costa, V. Shklover, L. Spiccia, G. B. Deacon, C. A. Bignozzi and M. Grätzel, *J. Am. Chem. Soc.*, 2001, **123**, 1613.
17. J. H. Heo, S. H. Im, J. H. Noh, T. N. Mandal, C.-S. Lim, J. A. Chang, Y. H. Lee, H.-J. Kim, A. Sarkar, M. K. Nazeeruddin, M. Gratzel and S. I. Seok, *Nature Photon.*, 2013, **7**, 486-491.
18. G. E. Eperon, S. D. Stranks, C. Menelaou, M. B. Johnston, L. M. Herz and H. J. Snaith, *Energy Environ. Sci.*, 2014, **7**, 982-988.
19. N. J. Jeon, J. H. Noh, Y. C. Kim, W. S. Yang, S. Ryu and S. I. Seok, *Nat. Mater.*, 2014, **13**, 897-903.
20. L. Han, A. Islam, H. Chen, C. Malapaka, B. Chiranjeevi, S. Zhang, X. Yang and M. Yanagida, *Energy Environ. Sci.*, 2012, **5**, 6057.
21. Y. Numata, S. P. Singh, A. Islam, M. Iwamura, A. Imai, K. Nozaki and L. Han, *Adv. Funct. Mater.*, 2013, **23**, 1817.
22. S.-H. Yang, K.-L. Wu, Y. Chi, Y.-M. Cheng and P.-T. Chou, *Angew. Chem. Int. Ed.*, 2011, **50**, 8270.
23. M. Kimura, J. Masuo, Y. Tohata, K. Obuchi, N. Masaki, T. N. Murakami, N. Koumura, K. Hara, A. Fukui, R. Yamanaka and S. Mori, *Chem. Eur. J.*, 2013, **19**, 1028.
24. P. T. Nguyen, R. Degn, H. T. Nguyen and T. Lund, *Sol. Energy Mater. Sol. Cells*, 2009, **93**, 1939.
25. C.-W. Hsu, S.-T. Ho, K.-L. Wu, Y. Chi, S.-H. Liu and P.-T. Chou, *Energy Environ. Sci.*, 2012, **5**, 7549.
26. H. Ozawa, S. Honda, D. Katano, T. Sugiura and H. Arakawa, *Dalton Trans.*, 2014, **43**, 8026-8036.
27. C.-C. Chou, K.-L. Wu, Y. Chi, W.-P. Hu, S. J. Yu, G.-H. Lee, C.-L. Lin and P.-T. Chou, *Angew. Chem. Int. Ed.*, 2011, **50**, 2054.
28. B. Schulze, D. G. Brown, K. C. D. Robson, C. Friebe , M. Jäger , E. Birckner, C. P. Berlinguette and U. S. Schubert *Chem. Eur. J.*, 2013, **19**, 14171.

29. C.-C. Chou, F.-C. Hu, H.-H. Yeh, H.-P. Wu, Y. Chi, J. N. Clifford, E. Palomares, S.-H. Liu, P.-T. Chou and G.-H. Lee, *Angew. Chem. Int. Ed.*, 2014, **53**, 178-183.
30. T. Privalov, G. Boschloo, A. Hagfeldt, P. H. Svensson and L. Kloo, *J. Phys. Chem. C*, 2009, **113**, 783.
31. F. Schiffmann, J. VandeVondele, J. Hutter, R. Wirz, A. Urakawa and A. Baiker, *J. Phys. Chem. C*, 2010, **114**, 8398.
32. M. Tuikka, P. Hirva, K. Rissanen, J. Korppi-Tommola and M. Haukka, *Chem. Commun.*, 2011, **47**, 4499.
33. H. Kusama, H. Sugihara and K. Sayama, *J. Phys. Chem. C*, 2011, **115**, 2544.
34. E. Mosconi, J.-H. Yum, F. Kessler, C. J. Gomez-Garcia, C. Zuccaccia, A. Cinti, M. K. Nazeeruddin, M. Grätzel and F. De Angelis, *J. Am. Chem. Soc.*, 2012, **134**, 19438.
35. A. Islam, F. A. Chowdhury, Y. Chiba, R. Komiya, N. Fuke, N. Ikeda, K. Nozaki and L. Han, *Chem. Mater.*, 2006, **18**, 5178.
36. K.-S. Chen, W.-H. Liu, Y.-H. Wang, C.-H. Lai, P.-T. Chou, G.-H. Lee, K. Chen, H.-Y. Chen, Y. Chi and F.-C. Tung, *Adv. Funct. Mater.*, 2007, **17**, 2964.
37. T. Funaki, M. Yanagida, N. Onozawa-Komatsuzaki, K. Kasuga, Y. Kawanishi and H. Sugihara, *Inorg. Chim. Acta*, 2009, **362**, 2519.
38. K. Chen, Y.-H. Hong, Y. Chi, W.-H. Liu, B.-S. Chen and P.-T. Chou, *J. Mater. Chem.*, 2009, **19**, 5329.
39. A. Hagfeldt, G. Boschloo, L. Sun, L. Kloo and H. Pettersson, *Chem. Rev.*, 2010, **110**, 6595.
40. J.-H. Yum, E. Baranoff, S. Wenger, M. K. Nazeeruddin and M. Grätzel, *Energy Environ. Sci.*, 2011, **4**, 842.
41. K.-L. Wu, J. N. Clifford, S.-W. Wang, Y. Aswani, E. Palomares, M. G. Lobello, E. Mosconi, F. De Angelis, W.-P. Ku, Y. Chi, M. K. Nazeeruddin and M. Grätzel, *ChemSusChem*, 2014, DOI: 10.1002/cssc.201402030.
42. B.-S. Chen, K. Chen, Y.-H. Hong, W.-H. Liu, T.-H. Li, C.-H. Lai, P.-T. Chou, Y. Chi and G.-H. Lee, *Chem. Commun.*, 2009, 5844.
43. T. Funaki, H. Funakoshi, O. Kitao, N. Onozawa-Komatsuzaki, K. Kasuga, K. Sayama and H. Sugihara, *Angew. Chem. Int. Ed.*, 2012, **51**, 7528.
44. S.-W. Wang, K.-L. Wu, E. Ghadiri, M. G. Lobello, S.-T. Ho, Y. Chi, J.-E. Moser, F. De Angelis, M. Grätzel and M. K. Nazeeruddin, *Chem. Sci.*, 2013, **4**, 2423.
45. Z.-S. Wang, T. Yamaguchi, H. Sugihara and H. Arakawa, *Langmuir*, 2005, **21**, 4272.
46. T. C. Wei, C. C. Wan and Y. Y. Wang, *Appl. Phys. Lett.*, 2006, **88**, 103122.
47. C.-C. Chou, F.-C. Hu, K.-L. Wu, T. Duan, Y. Chi, S.-H. Liu, G.-H. Lee and P.-T. Chou, *Inorg. Chem.*, 2014, **53**, 8593-8599.
48. S. Fantacci, E. Ronca and F. De Angelis, *J. Phys. Chem. Lett.*, 2013, **5**, 375-380.
49. P.-T. Chou, Y. Chi, M.-W. Chung and C.-C. Lin, *Coord. Chem. Rev.*, 2011, **255**, 2653.
50. N. Martsinovich and A. Troisi, *Energy Environ. Sci.*, 2011, **4**, 4473.
51. B. C. O'Regan, K. Walley, M. Juozapavicius, A. Anderson, F. Matar, T. Ghaddar, S. M. Zakeeruddin, C. Klein and J. R. Durrant, *J. Am. Chem. Soc.*, 2009, **131**, 3541.
52. A. Reynal, A. Forneli, E. Martinez-Ferrero, A. Sánchez-Díaz, A. n. Vidal-Ferran, B. C. O'Regan and E. Palomares, *J. Am. Chem. Soc.*, 2008, **130**, 13558.
53. K. C. D. Robson, K. Hu, G. J. Meyer and C. P. Berlinguette, *J. Am Chem. Soc.*, 2013, **135**, 1961.
54. Y. Cao, Y. Bai, Q. Yu, Y. Cheng, S. Liu, D. Shi, F. Gao and P. Wang, *J. Phys. Chem. C*, 2009, **113**, 6290.
55. H.-H. Yeh, S.-T. Ho, Y. Chi, J. N. Clifford, E. Palomares, S.-H. Liu and P.-T. Chou, *J. Mater. Chem. A*, 2013, **1**, 7681.
56. M. Planells, L. Pelleja, J. N. Clifford, M. Pastore, F. De Angelis, N. Lopez, S. R. Marder and E. Palomares, *Energy Environ. Sci.*, 2011, **4**, 1820.
57. A. Listorti, B. O'Regan and J. R. Durrant, *Chem. Mater.*, 2011, **23**, 3381.

58. A. Y. Anderson, P. R. F. Barnes, J. R. Durrant and B. C. O'Regan, *J. Phys. Chem. C*, 2011, **115**, 2439.
59. J. N. Clifford, E. Martinez-Ferrero and E. Palomares, *J. Mater. Chem.*, 2012, **22**, 12415.
60. K.-L. Wu, W.-P. Ku, J. N. Clifford, E. Palomares, S.-T. Ho, Y. Chi, S.-H. Liu, P.-T. Chou, M. K. Nazeeruddin and M. Grätzel, *Energy Environ. Sci.*, 2013, **6**, 859.
61. H. Ozawa, M. Awa, T. Ono and H. Arakawa, *Chem. Asian J.*, 2012, **7**, 156.
62. H. Ozawa, R. Shimizu and H. Arakawa, *RSC Adv.*, 2012, **2**, 3198.
63. H. Ozawa, Y. Okuyama and H. Arakawa, *ChemPhysChem*, 2014, **15**, 1201-1206.
64. A. Reynal, A. Forneli and E. Palomares, *Energy Environ. Sci.*, 2010, **3**, 805.
65. J. N. Clifford, E. Palomares, M. K. Nazeeruddin, M. Grätzel and J. R. Durrant, *J. Phys. Chem. C*, 2007, **111**, 6561.
66. K.-L. Wu, C.-H. Li, Y. Chi, J. N. Clifford, L. Cabau, E. Palomares, Y.-M. Cheng, H.-A. Pan and P.-T. Chou, *J. Am. Chem. Soc.*, 2012, **134**, 7488.
67. J. Bisquert, M. Grätzel, Q. Wang and F. Fabregat-Santiago, *J. Phys. Chem. B*, 2006, **110**, 11284-11290.
68. F. Sauvage, S. Chhor, A. Marchioro, J.-E. Moser and M. Grätzel, *J. Am. Chem. Soc.*, 2011, **133**, 13103.